Journal of Applied Physics

Janus two-dimensional materials based on group IV monochalcogenides

Cite as: J. Appl. Phys. **128**, 045115 (2020); https://doi.org/10.1063/5.0012427
Submitted: 30 April 2020 . Accepted: 17 July 2020 . Published Online: 29 July 2020

Leandro Seixas

Journal of Applied Physics ARTICLE scitation.org/journal/jap

Janus two-dimensional materials based on group IV monochalcogenides

Cite as: J. Appl. Phys. **128**, 045115 (2020); doi: 10.1063/5.0012427
Submitted: 30 April 2020 · Accepted: 17 July 2020 ·
Published Online: 29 July 2020

Leandro Seixas[a)]

AFFILIATIONS

MackGraphe—Graphene and Nanomaterials Research Center, Mackenzie Presbyterian University, Rua da Consolação 896, São Paulo, SP 01302-907, Brazil and School of Engineering, Mackenzie Presbyterian University, Rua da Consolação 896, São Paulo, SP 01302-907, Brazil

Note: This paper is part of the Special Topic on Beyond Graphene: Low Symmetry and Anisotropic 2D Materials.
[a)]**Author to whom correspondence should be addressed:** leandro.seixas@mackenzie.br

ABSTRACT

The discovery and design of two-dimensional (2D) materials has aided the development of novel nanoscale devices for various applications. Here, we show the structural, electronic, and vibrational properties of 15 2D materials based on Janus substitution (atomic layer substitution) of group IV monochalcogenides. Although group IV monochalcogenides have already been extensively studied because of their very promising piezoelectric and thermoelectric properties, these Janus materials appear as potential candidates for similar applications but with a broken symmetry that can enrich their electronic and optical properties and the coupling of these with other physical properties. Based on first-principles calculations, we investigate the stability of the Janus materials according to energetic, dynamical, and mechanical criteria. Understanding of the physical properties of these 2D materials can provide guidance for the development of novel nanoscale electronic devices.

I. INTRODUCTION

Two-dimensional (2D) materials are a class of materials of great interest to the scientific community owing to the new physical phenomena that they exhibit, as well as their potential technological applications. Since the discovery of graphene in 2004,[1,2] several other 2D materials have emerged with a variety of electronic, optical, magnetic, and piezoelectric properties. These novel materials include transition metal dichalcogenides (TMDs), among which MoS_2 is one of the best-known examples.[3–5] They also include 2D materials such as black phosphorus (BP),[6–10] a direct-bandgap semiconductor formed from just phosphorus atoms in a puckered geometry, and the group IV monochalcogenides, which are isoelectronic to BP.[11–13] These 2D group IV monochalcogenides include compounds such as GeS, GeSe, GeTe, SnS, SnSe, and SnTe. They have interesting electronic properties, with direct-to-indirect gap transitions with the number of layers. They also have high figures of merit (ZT) for thermoelectric effects[10,14] and high piezoelectric coefficients.[12,13]

The piezoelectric properties of 2D materials are very interesting because of their prospective use in energy nanogenerators for wearable and implantable devices. The piezoelectric materials that are presently available are lead-based perovskite materials. However, if such materials were to be used in wearable or implantable devices, there would be the risk of lead poisoning, and therefore, there is a need to find novel piezoelectric materials that do not contain toxic elements. In addition to flexible and wearable electronics applications, 2D materials form a good platform for discovering new materials with atomic-scale manipulation, including piezoelectric materials. For a material to exhibit piezoelectricity, it must have no inversion symmetry.[15,16] Piezoelectricity has recently been observed in MoS_2 monolayers, and this property has been applied in an energy nanogenerator.[17] Group IV monochalcogenides have also been studied, owing to their piezoelectric properties as monolayers. In fact, the piezoelectric constants of a SnSe monolayer have been calculated to be as high as $d_{11} = 250\,\mathrm{pm/V}$, which is almost two orders of magnitude larger than the piezoelectric constants found in MoS_2.[18–20] These giant piezoelectric constants make these materials very promising for applications in atomic-scale piezoelectric devices.

One way to break symmetry is to replace an atomic sublayer with elements of the same chemical group, in what is known as

Janus substitution. The first Janus 2D material studied was MoSSe.[21–23] To produce this material, a sublayer of the starting material (MoS_2) was removed by an H_2 plasma. In the next step, another element (Se) was thermally grown over the sample in a process known as selenization.[21] The resulting MoSSe material has a sulfur underlay on one side (bottom) and selenium on the other side (top). This symmetry breaking results in a vertical piezoelectric constant (d_{31}), in contrast to what is found in MoS_2, where the electrical polarization is in the basal plane, in the same direction as strain (d_{11}). This MoSSe vertical piezoelectricity has been experimentally observed through piezoresponse measurements in atomic force microscopy. Other Janus 2D materials are also being studied owing to their unique electronic properties, piezoelectricity, and even second-harmonic generation.[24]

Here, we describe the electronic, vibrational, and mechanical properties of Janus 2D materials based on group IV monochalcogenides. The vibrational and mechanical properties will be studied to determine the stability of these 2D materials. Owing to the geometry of the parent compounds (Ge_2S_2, Ge_2Se_2, Ge_2Te_2, Sn_2S_2, Sn_2Se_2, and Sn_2Te_2), there are three ways to perform Janus substitutions on these materials: (1) replacing a chalcogen (S, Se, or Te) on one side, resulting in a ternary material denoted here as type TA; (2) replacing a crystallogen (Ge or Sn) on one side, resulting in a ternary material denoted as type TB; and (3) replacing both a chalcogen and a crystallogen, resulting in a quaternary material denoted as type Q. In total, 15 2D materials will be studied here: six type TA (Ge_2SSe, Ge_2STe, Ge_2SeTe, Sn_2SSe, Sn_2STe, and Sn_2SeTe), three type TB ($GeSnS_2$, $GeSnSe_2$, and $GeSnTe_2$), and six type Q (GeS/SnSe, GeS/SnTe, GeSe/SnS, GeSe/SnTe, GeTe/SnS, and GeTe/SnSe). Schematic representations of these three types of Janus 2D materials are depicted in Fig. 1.

II. METHODS

The atomistic simulations were performed via *ab initio* methods based on density functional theory (DFT).[25–27] The calculations were carried out using the SIESTA code, which implements DFT with localized numerical atomic orbitals.[28] We used a norm-conserved pseudopotential formalism with the Troullier–Martins method.[29] The exchange-correlation functional used was in the generalized gradient approximation, with Perdew–Burke–Ernzerhof (PBE) parameterization.[30] k-point sampling in the Brillouin zone was performed using the Moreno–Soler algorithm,[31] with a cutoff radius of 20 Å for geometry optimizations and electronic band structure calculations. Densities of states (DOS) were calculated with a Monkhorst–Pack algorithm grid of $200 \times 200 \times 1$ and a Gaussian smearing of 0.04 eV.[32] Simulation parameters also included a mesh cutoff of 400 Ry, a double-ζ basis with

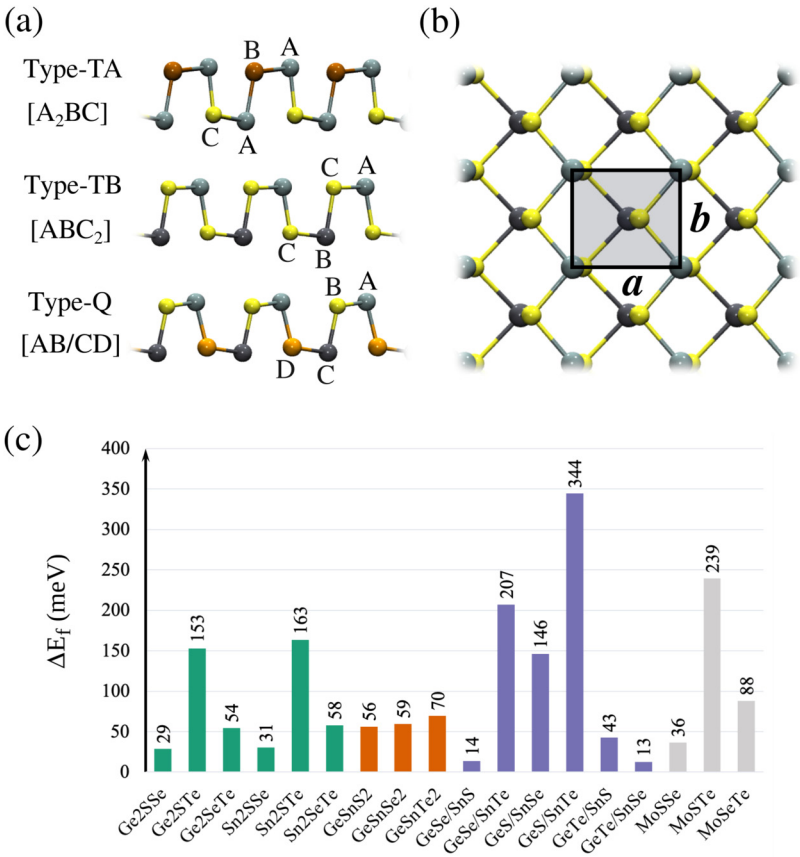

FIG. 1. (a) Ball-and-stick representations of Janus group IV monochalcogenides of types TA, TB, and Q. (b) Top view of Janus group IV monochalcogenides. (c) Formation energy per unit cell relative to the two parent compounds.

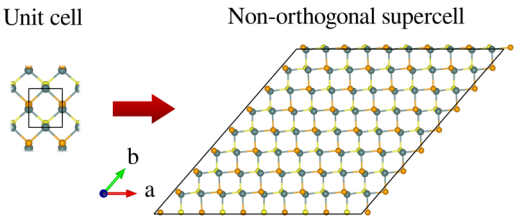

FIG. 2. Schematic representation of a non-orthogonal supercell used in the finite-displacement method for phonon calculations.

polarization orbitals (DZP), and an energy shift of 0.03 eV. All geometries were relaxed with forces smaller than 0.001 eV/Å and stresses smaller than 0.003 GPa.

Phonon dispersions were calculated using the PHONOPY tool,[33] with SIESTA as the force set calculator. These forces were calculated with atomic displacements in a non-orthogonal supercell, given by the nondiagonal matrix

$$M = \begin{pmatrix} 5 & 8 & 0 \\ -5 & 0 & 0 \\ 0 & 0 & 1 \end{pmatrix}. \quad (1)$$

These non-orthogonal supercells were used to provide a better calculation of acoustic modes in the chemical bond directions in the 2D materials. A schematic representation of such a supercell is depicted in Fig. 2. This non-orthogonal supercell has $\det(M) = 40$ more atoms in the unit cell than in the primitive unit cell.

The formation energy for the Janus group IV monochalcogenide AB/CD, with a crystallogen A and a chalcogen B in the top moiety and a crystallogen C and a chalcogen D in the bottom moiety, is given by

$$\Delta E_f = E_{\text{tot}}[AB/CD] - \frac{1}{2}E_{\text{tot}}[A_2B_2] - \frac{1}{2}E_{\text{tot}}[C_2D_2], \quad (2)$$

where $E_{\text{tot}}[X]$ is the total energy of material X and A_2B_2 and C_2D_2 are the group IV monochalcogenide parent compounds (Ge_2S_2, Ge_2Se_2, Ge_2Te_2, Sn_2S_2, Sn_2Se_2, or Sn_2Te_2). Low formation energies indicate greater ease of synthesizing these materials.

III. RESULTS AND DISCUSSION

Figure 1(a) depicts side views of ball-and-stick representations of the puckered geometry of Janus group IV monochalcogenides. From these side views, it is possible to define the top and bottom moieties as the sublayers with a crystallogen (Ge or Sn) and a chalcogen (S, Se, or Te). These 2D materials are classified here as type TA for ternary compounds with top and bottom moieties with the same crystallogen but different chalcogens, as type TB for ternary compounds with a similar geometry but the same chalcogen and a different crystallogen and as type Q for quaternary compounds with different crystallogens and chalcogens for both top and bottom moieties. A top view of a type TB Janus material is depicted in Fig. 1(b). The lattice constants a and b for each material are shown in Table I. The anisotropy parameter a/b is larger for lighter materials and smaller for heavier materials. The lattice constants a and b can also be compared with the averages of the lattice constants of the parent compounds, $\bar{a}$ and $\bar{b}$, also shown in Table I. For a more stable material such as Ge_2SSe, the calculated lattice constants are very close to the averages of the GeS and GeSe lattice constants, whereas for the Janus GeS/SnTe, the calculated lattice constant a is considerably larger than the average $\bar{a}$ of the GeS and SnTe lattice constants: $a = 5.01$ Å compared with $\bar{a} = 4.62$ Å. From a comparison of the lattice constants a and b of the Janus materials with the average of each lattice constant of the parent compounds, it can be seen that the lattice constant b is always very close to the average, whereas the lattice constant a exhibits a discrepancy for some Janus materials. For example, the lattice constant a of Ge_2SSe shows a variation of less than 1% compared with the average $\bar{a}$ of the lattice constants of the parent compounds GeS and GeSe, whereas the corresponding variation in a for the Janus material GeS/SnTe compared with $\bar{a}$ for the parent compounds GeS and SnTe reaches 8.6%. This large variation compared with the average may indicate an instability of the Janus material GeS/SnTe.

The formation energies of the Janus materials and parent compounds are shown in Fig. 1(c). In this plot, type TA are in green, type TB in orange, and type Q in purple. The formation energies calculated in this work for the Janus TMDs MoSSe, MoSTe, and MoSeTe are shown in gray for comparison purposes. We can see that Janus materials such as Ge_2SSe, Sn_2SSe, GeSe/SnS, and GeTe/SnSe have lower formation energies than the already known Janus material MoSSe. These low formation energies were

TABLE I. Lattice constants a and b, anisotropy parameter a/b, and bandgap ΔE_g of group IV monochalcogenides and Janus 2D materials based on them. $\bar{a}$ and $\bar{b}$ are the averages of the lattice constants of the two parent compounds.

Material	a (Å)	b (Å)	a/b	$\bar{a}$	$\bar{b}$	ΔE_g (eV)
Ge_2S_2	4.51	3.69	1.222	…	…	1.61
Ge_2Se_2	4.39	3.99	1.099	…	…	1.17
Ge_2Te_2	4.48	4.28	1.047	…	…	0.91
Sn_2S_2	4.38	4.10	1.068	…	…	1.30
Sn_2Se_2	4.55	4.31	1.056	…	…	0.91
Sn_2Te_2	4.73	4.60	1.027	…	…	0.64
Ge_2SSe	4.47	3.84	1.163	4.45	3.84	1.32
Ge_2STe	4.53	4.03	1.123	4.50	3.99	0.97
Ge_2SeTe	4.47	4.14	1.079	4.44	4.14	0.88
Sn_2SSe	4.51	4.20	1.074	4.47	4.21	1.06
Sn_2STe	4.77	4.33	1.100	4.56	4.35	0.76
Sn_2SeTe	4.70	4.45	1.055	4.64	4.46	0.69
$GeSnS_2$	4.49	3.88	1.158	4.45	3.90	1.27
$GeSnSe_2$	4.60	4.11	1.119	4.47	4.15	0.98
$GeSnTe_2$	4.70	4.43	1.061	4.61	4.44	0.76
GeS/SnSe	4.75	3.94	1.207	4.53	4.00	0.96
GeS/SnTe	5.01	4.10	1.221	4.62	4.15	0.69
GeSe/SnS	4.45	4.03	1.105	4.39	4.05	1.15
GeSe/SnTe	4.86	4.24	1.147	4.56	4.30	0.73
GeTe/SnS	4.49	4.21	1.067	4.43	4.19	0.83
GeTe/SnSe	4.54	4.30	1.055	4.52	4.30	0.78

the first evidence of stability for some 2D Janus group IV monochalcogenides. Materials with higher formation energies, such as GeS/SnTe, will be harder to form and stabilize. The formation energies were calculated relative to the averages of the total energies of the parent compounds. For example, the formation energy for the Ge_2SSe was calculated as the total energy $E_{tot}[Ge_2SSe]$ minus the average of the total energies of the two parent compounds $E_{tot}[Ge_2S_2]$ and $E_{tot}[Ge_2Se_2]$.

A. Electronic properties

The electronic properties of these Janus materials were investigated using an electronic band structure with orbital projections (fatbands) and projected density of states (PDOS). Figure 3 shows the electronic band structures for ternary Janus materials (type TA and type TB). The band structures are plotted in the high-symmetry paths $\Gamma-X$ in the armchair direction and $\Gamma-Y$ in the zigzag directions. These paths between high-symmetry k-points are associated with the lattice constants a and b, as shown in Fig. 1(a). Projections on the light elements are shown in blue and projections on heavy elements in red. For the PDOS, projections on light, heavy, and host elements in Janus materials are shown in blue, red, and gray, respectively. The host elements are those that are kept the same in both moieties and parent compounds. For example, for the type TA Ge_2SSe, Ge is the host element, S the light element, and Se the heavy element. For the type TB $GeSnS_2$, S is the host element, Ge the light element, and Sn the heavy element. The PDOS are shown as stacked area plots. The electronic properties for type TA are shown from Figs. 3(a) to 3(f) and those for type TB from Figs. 3(g) to 3(i). All these materials are semiconductors with an indirect bandgap from $\Delta E_g = 0.69$ eV (Sn_2SeTe) to $\Delta E_g = 1.32$ eV (Ge_2SSe). It must be kept in mind that the calculated bandgaps ΔE_g

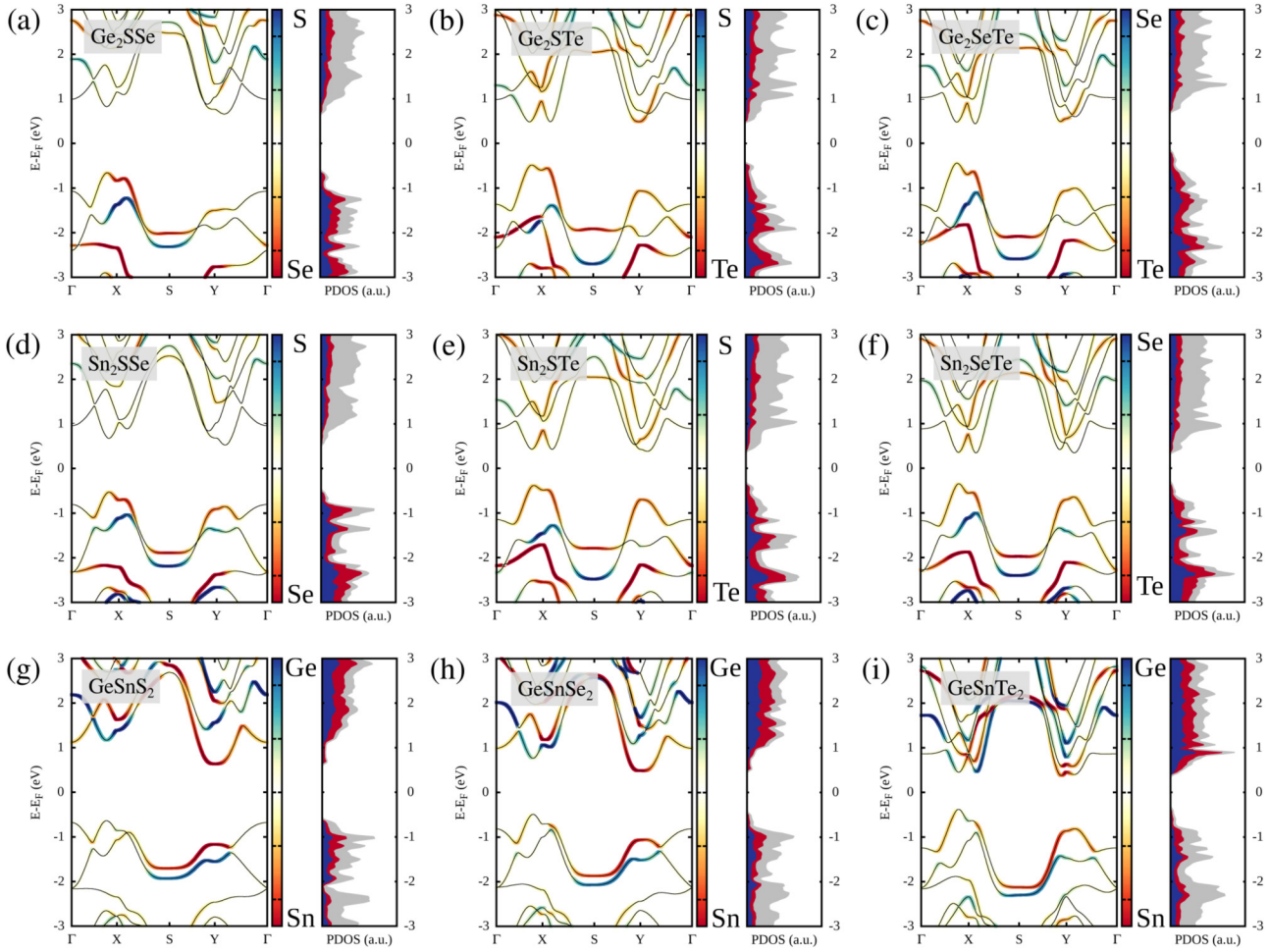

FIG. 3. Electronic band structure and projected density of states (PDOS) of ternary (type TA and type TB) Janus group IV monochalcogenides: (a) Ge_2SSe, (b) Ge_2STe, (c) Ge_2SeTe, (d) Sn_2SSe, (e) Sn_2STe, (f) Sn_2SeTe, (g) $GeSnS_2$, (h) $GeSnSe_2$, and (i) $GeSnTe_2$. The color maps show orbital projections from the lighter element (in blue) to the heavier element (in red). The PDOS for the lighter and heavier elements are in blue and red, respectively, and those for the host elements are in light gray.

are usually underestimated by the PBE functional.[30] The valleys and hills in the conduction and valence bands are very similar to those found in the parent compounds, enabling potential valleytronic effects.[34] For type TA, the valence band maxima (VBM) are mostly composed of heavy elements, and the conduction band minima (CBM) are mostly composed of host elements (Ge or Sn). For type TB, the VBM are mostly composed of host elements (S, Se, or Te), and the CBM are mostly composed of the heavy element (Sn).

Figure 4 shows the electronic band structures and PDOS of type Q Janus materials. In these cases, the projections were made on top moieties (AB) and bottom moieties (CD), as labeled in Fig. 1(a). There are no host elements in these Janus materials. For both band structures and PDOS, projections on the top moieties are shown in blue and those on the bottom moieties in red. The PDOS are also shown as stacked area plots. All type Q Janus materials are semiconductors with indirect bandgaps ranging from 0.69 eV (GeS/SnTe) to 1.15 eV (GeSe/SnS). These type Q Janus materials exhibit an interesting phenomenon related to the band edges. For GeS/SnSe, GeS/SnTe, and GeSe/SnTe, both VBM and CBM are in the same bottom moiety (those with Sn). The electronic band structures of these materials are shown in Figs. 4(a)–4(c). These three materials also have the highest formation energies in the type Q class. However, for GeSe/SnS, GeTe/SnS, and GeTe/SnSe, the VBM and CBM are in opposite moieties. The CBM is in the bottom moiety (those with Sn) and the VBM is in the top moiety (those with Ge). The electronic band structures of these materials are shown in Figs. 4(d)–4(f). This separation of the band edges in different sublayers (moieties) may have interesting implications for electron–hole separation, resulting in low recombination rates. Also, these materials have the lowest formation energies in the type Q class, including $\Delta E_f = 13\,\mathrm{meV/cell}$ for GeTe/SnSe, which is lower than the formation energy of MoSSe. Usually, the CBM and VBM are close to X and Y points in the Brillouin zone, with bands with a camel hump shape around these points. For GeTe/SnS, the bands are very close to a direct bandgap, increasing the optical absorption of this material.

B. Vibrational properties and dynamical stability

To investigate the dynamical stability of these 15 2D materials, the phonon band structures were calculated using non-orthogonal supercells (see Sec. II). Stability was indicated by the absence of imaginary frequencies in acoustic branches. However, owing to the low symmetry of these materials, small parabolic valleys appeared in the phonon calculations. The presence of these small valleys is not related to the stability of the material but is due to numerical errors caused by the finiteness of the supercells. These small valleys have even been observed experimentally in stable 2D materials.[35] The use of non-orthogonal supercells reduced this effect but did not completely eliminate it. Phonon calculations with slightly smaller and larger supercells also exhibit this effect. On this basis, a soft threshold of $10i\,\mathrm{cm}^{-1}$ is proposed as a stability criterion. Imaginary frequencies higher (in absolute value) than this threshold may indicate an instability of the Janus material. Making use of this soft stability criterion, all ternary Janus materials (type TA and

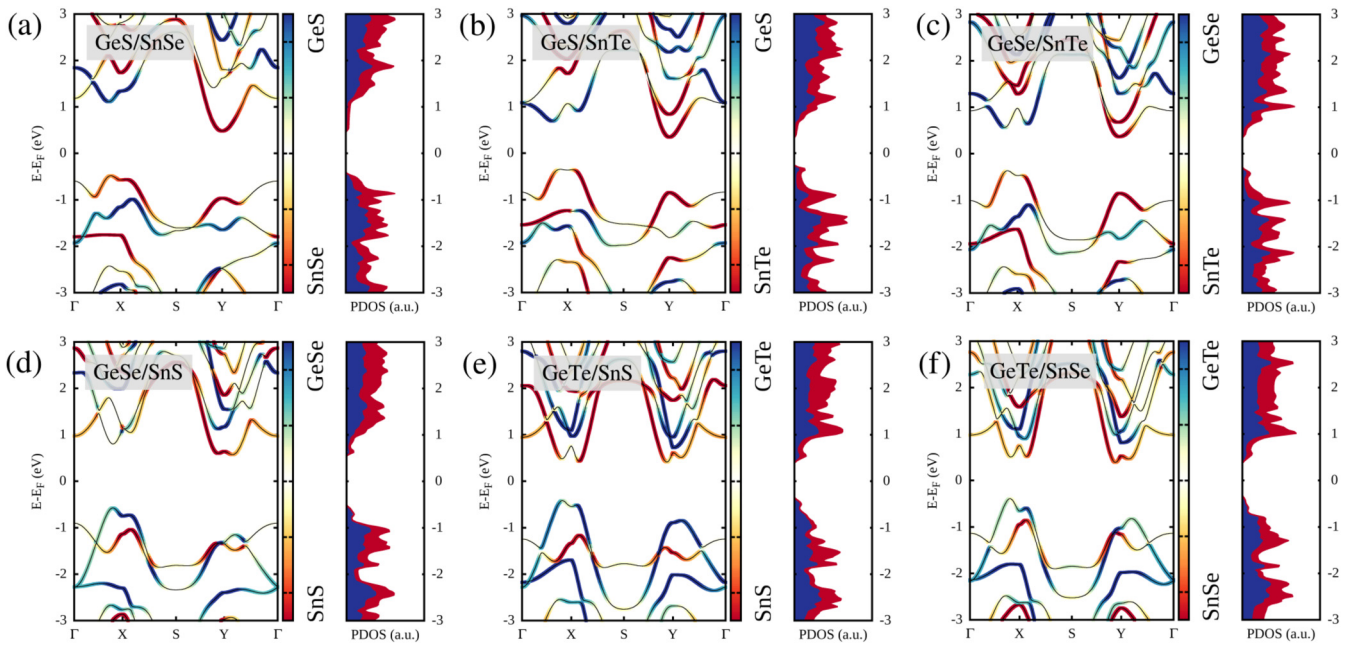

FIG. 4. Electronic band structure and projected density of states (PDOS) of quaternary (type Q) Janus group IV monochalcogenides: (a) GeS/SnSe, (b) GeS/SnTe, (c) GeSe/SnTe, (d) GeSe/SnS, (e) GeTe/SnS, and (f) GeTe/SnSe. The color maps show orbital projections of the top moiety (in blue) and the bottom moiety (in red). The PDOS for the top and bottom moieties are shown in blue and red, respectively.

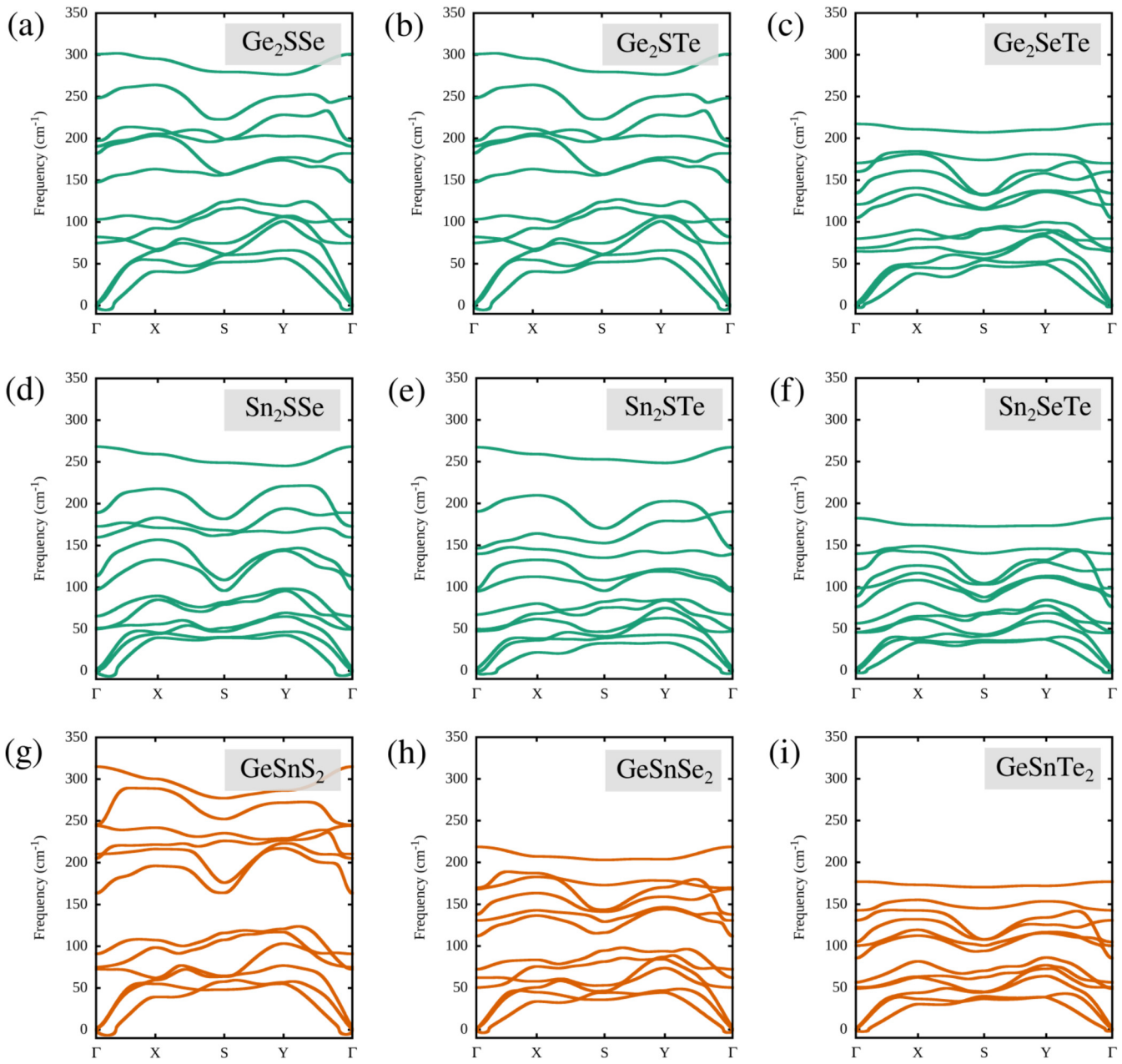

FIG. 5. Phonon band structure for ternary (type TA and type TB) Janus group IV monochalcogenides: (a) Ge_2SSe, (b) Ge_2STe, (c) Ge_2SeTe, (d) Sn_2SSe, (e) Sn_2STe, (f) Sn_2SeTe, (g) $GeSnS_2$, (h) $GeSnSe_2$, and (i) $GeSnTe_2$. The band structures of the type TA and type TB monochalcogenides are shown in green and orange, respectively.

type TB) ought to exhibit dynamical stability, as shown in Fig. 5. It should be noted that as the small imaginary frequencies occur in the flexural acoustic modes, interactions with substrates should increase the stability of the material. In the plots, imaginary frequencies are shown as negative values.

For the type Q Janus monochalcogenides, the phonon dispersions were also calculated, as shown in Fig. 6. The material GeS/SnTe showed low stability, as indicated by the presence of imaginary values for the flexural acoustic mode greater than $10i\,\mathrm{cm}^{-1}$. This imaginary mode was also not restricted to the vicinity of the Γ point

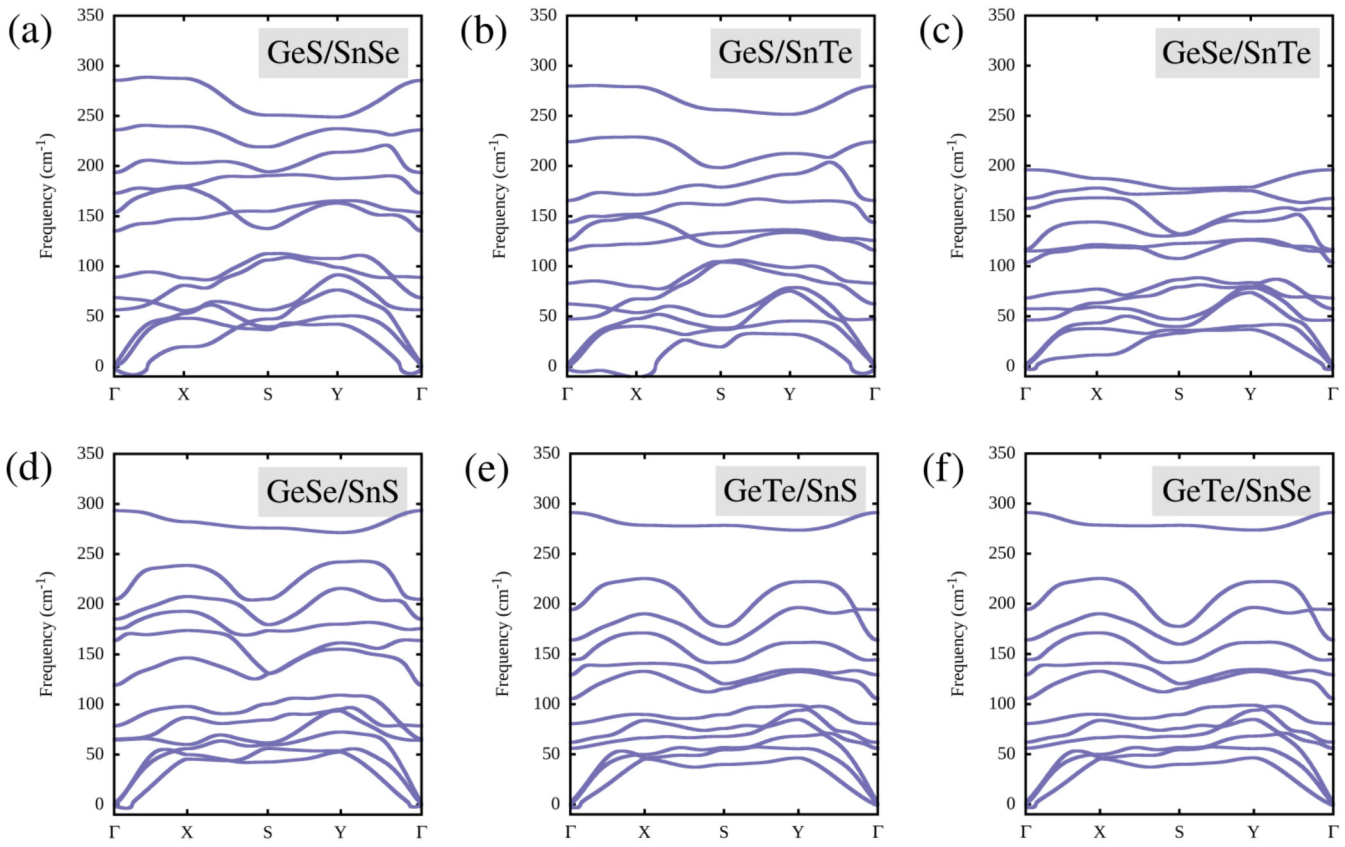

FIG. 6. Phonon band structure for quaternary (type Q) Janus group IV monochalcogenides: (a) GeS/SnSe, (b) GeS/SnTe, (c) GeSe/SnTe, (d) GeSe/SnS, (e) GeTe/SnS, and (f) GeTe/SnSe.

(large phonon wavelength) and had greater instability at the X point (armchair). This instability at the X point could indicate a Peierls distortion along this direction. However, when we calculated the structural properties with a cell doubled in the x direction, we could not observe any distortion in the lattice, and the new phonon dispersion also had imaginary modes greater than $10i\,\mathrm{cm}^{-1}$. From this phonon dispersion, we have evidence of dynamical instability of the type Q Janus material GeS/SnTe. The other type Q Janus materials exhibited dynamical stability similar to the type TA and type TB materials.

C. Mechanical properties

A third stability criterion was employed in the analysis of the materials through the convexity of the internal energy with strain. Varying the lattice constants a and b independently, as shown in Fig. 7(a), we can calculate the elastic energy density,

$$\Delta U(\varepsilon_x, \varepsilon_y) = \frac{U(\varepsilon_x, \varepsilon_y) - U(0,0)}{A_0}, \tag{3}$$

where A_0 is the area of the unstrained unit cell, $\varepsilon_x = (a - a_0)/a_0$, $\varepsilon_y = (b - b_0)/b_0$, and a_0 and b_0 are the lattice constants of the unstrained unit cell. Applying strains from -5% to $+5\%$, in steps of 1%, we obtain a 2D surface. This surface can be fitted by the quadratic polynomial,

$$\Delta U(\varepsilon_x, \varepsilon_y) = \frac{1}{2}C_{11}\varepsilon_x^2 + \frac{1}{2}C_{22}\varepsilon_y^2 + C_{12}\varepsilon_x\varepsilon_y. \tag{4}$$

Based on this curve fit, we obtain the elastic constants C_{11}, C_{22}, and C_{12}, using the Voigt notation. We can see from Fig. 7(b) that the elastic constants C_{22} are usually much larger than the constants C_{11} and C_{12}, indicating greater rigidity in the y direction (zigzag). The large anisotropy observed in the elastic constants is similar to previous results for black phosphorus and group IV monochalcogenides.[13,36]

The observation that the elastic constants are positive indicates that the Janus group IV monochalcogenides are mechanically stable under small planar deformations. In addition to the stability criteria from cohesive energies (energetic stability) and acoustic phonon modes (dynamical stability), this criterion confirms the stability of these 2D materials expected at the start of this work.

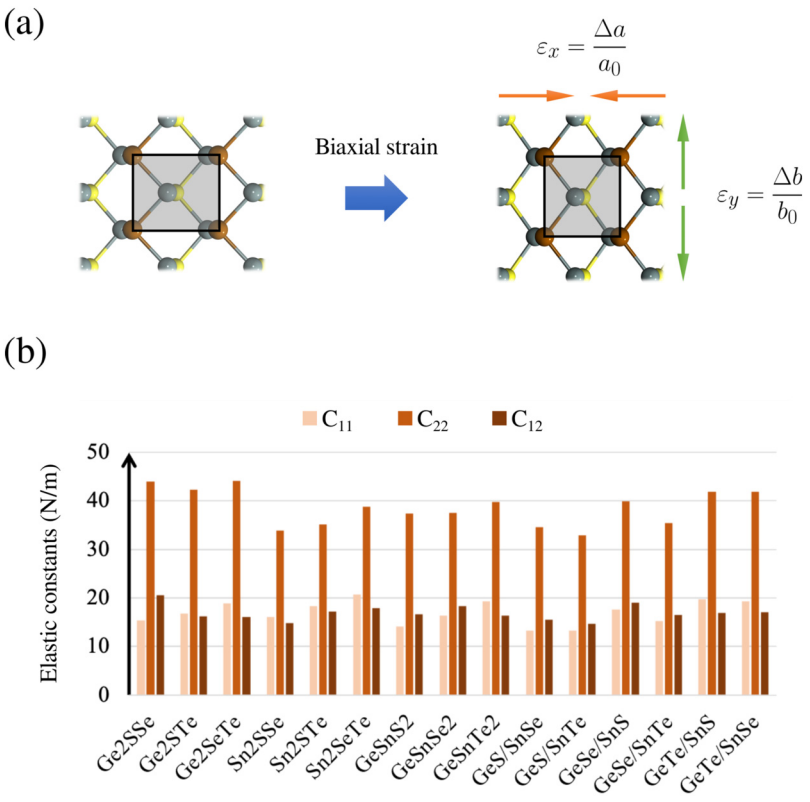

FIG. 7. (a) Schematic representation of biaxial strains ε_x and ε_y of a Janus group IV monochalcogenide material. (b) Elastic constants C_{11}, C_{22}, and C_{21} (in N/m) of the 15 Janus group IV monochalcogenides.

IV. CONCLUSION

We have investigated the structural, electronic, and vibrational properties of 15 2D materials constructed through Janus substitutions in group IV monochalcogenides. These 2D materials are stable according to criteria based on cohesive energy (energetic stability), positivity of acoustic branches (dynamical stability), and positivity of elastic constants (mechanical stability). One of the materials, GeS/SnTe, proves to be an exception with regard to stability since it exhibits possible dynamic instability. All of these 2D materials are semiconductors with an indirect bandgap. The orbital compositions of the VBM and CBM are strongly correlated with the type of Janus substitution (TA, TB, or Q). The symmetry breaking induced by the Janus substitution allows the creation of vertical electrical polarizations in the basal plane of the materials, resulting in nonzero piezoelectric constants.

ACKNOWLEDGMENTS

The author acknowledges financial support from the MackPesquisa, the Conselho Nacional de Desenvolvimento Científico e Tecnológico (CNPq) (Grant Nos. 306422/2017-4 and 40825/2018-5), the Fundação de Amparo à Pesquisa do Estado de São Paulo (FAPESP) (Grant No. 2017/00486-1), and the high-performance computing facilities of LoboCarneiro/NACAD/UFRJ.

DATA AVAILABILITY

The data that support the findings of this study are openly available in GitHub at https://github.com/SeixasResearch/JanusData.git, Ref. 37.

REFERENCES

[1]K. S. Novoselov, A. K. Geim, S. V. Morozov, D. Jiang, Y. Zhang, S. V. Dubonos, I. V. Grigorieva, and A. A. Firsov, Science **306**, 666 (2004).
[2]A. H. Castro Neto, F. Guinea, N. Peres, K. Novoselov, and A. Geim, Rev. Mod. Phys. **81**, 109 (2009).
[3]K. F. Mak, C. Lee, J. Hone, J. Shan, and T. F. Heinz, Phys. Rev. Lett. **105**, 136805 (2010).
[4]B. Radisavljevic, A. Radenovic, J. Brivio, V. Giacometti, and A. Kis, Nat. Nanotechnol. **6**, 147 (2011).
[5]S. Manzeli, D. Ovchinnikov, D. Pasquier, O. V. Yazyev, and A. Kis, Nat. Rev. Mater. **2**, 17033 (2017).
[6]L. Li, Y. Yu, G. J. Ye, Q. Ge, X. Ou, H. Wu, D. Feng, X. H. Chen, and Y. Zhang, Nat. Nanotechnol. **9**, 372 (2014).
[7]H. Liu, A. T. Neal, Z. Zhu, Z. Luo, X. Xu, D. Tománek, and P. D. Ye, ACS Nano **8**, 4033 (2014).
[8]A. S. Rodin, A. Carvalho, and A. H. Castro Neto, Phys. Rev. Lett. **112**, 176801 (2014).
[9]S. P. Koenig, R. A. Doganov, H. Schmidt, A. Castro Neto, and B. Özyilmaz, Appl. Phys. Lett. **104**, 103106 (2014).
[10]A. Carvalho, M. Wang, X. Zhu, A. S. Rodin, H. Su, and A. H. Castro Neto, Nat. Rev. Mater. **1**, 16061 (2016).
[11]L. C. Gomes and A. Carvalho, Phys. Rev. B **92**, 085406 (2015).

[12]L. C. Gomes, A. Carvalho, and A. H. Castro Neto, Phys. Rev. B **92**, 214103 (2015).
[13]R. Fei, W. Li, J. Li, and L. Yang, Appl. Phys. Lett. **107**, 173104 (2015).
[14]L.-D. Zhao, S.-H. Lo, Y. Zhang, H. Sun, G. Tan, C. Uher, C. Wolverton, V. P. Dravid, and M. G. Kanatzidis, Nature **508**, 373 (2014).
[15]R. E. Newnham, *Properties of Materials* (Oxford University Press, 2015).
[16]M. Tinkham, *Group Theory and Quantum Mechanics* (McGraw-Hill, 1964).
[17]W. Wu and Z. L. Wang, Nat. Rev. Mater. **1**, 16031 (2016).
[18]K.-A. N. Duerloo, M. T. Ong, and E. J. Reed, J. Phys. Chem. Lett. **3**, 2871 (2012).
[19]W. Wu, L. Wang, Y. Li, F. Zhang, L. Lin, S. Niu, D. Chenet, X. Zhang, Y. Hao, T. F. Heinz *et al.*, Nature **514**, 470 (2014).
[20]H. Zhu, Y. Wang, J. Xiao, M. Liu, S. Xiong, Z. J. Wong, Z. Ye, Y. Ye, X. Yin, and X. Zhang, Nat. Nanotechnol. **10**, 151 (2015).
[21]A.-Y. Lu, H. Zhu, J. Xiao, C.-P. Chuu, Y. Han, M.-H. Chiu, C.-C. Cheng, C.-W. Yang, K.-H. Wei, Y. Yang *et al.*, Nat. Nanotechnol. **12**, 744 (2017).
[22]J. Zhang, S. Jia, I. Kholmanov, L. Dong, D. Er, W. Chen, H. Guo, Z. Jin, V. B. Shenoy, L. Shi *et al.*, ACS Nano **11**, 8192 (2017).
[23]L. Dong, J. Lou, and V. B. Shenoy, ACS Nano **11**, 8242 (2017).
[24]Y. Wei, X. Xu, S. Wang, W. Li, and Y. Jiang, Phys. Chem. Chem. Phys. **21**, 21022 (2019).
[25]P. Hohenberg and W. Kohn, Phys. Rev. **136**, B864 (1964).
[26]W. Kohn and L. J. Sham, Phys. Rev. **140**, A1133 (1965).
[27]K. Capelle, Braz. J. Phys. **36**, 1318 (2006).
[28]A. García, N. Papior, A. Akhtar, E. Artacho, V. Blum, E. Bosoni, P. Brandimarte, M. Brandbyge, J. Cerdá, F. Corsetti *et al.*, J. Chem. Phys. **152**, 204108 (2020).
[29]N. Troullier and J. L. Martins, Phys. Rev. B **43**, 1993 (1991).
[30]J. Perdew, K. Burke, and M. Ernzerhof, Phys. Rev. Lett. **77**, 3865 (1996).
[31]J. Moreno and J. M. Soler, Phys. Rev. B **45**, 13891 (1992).
[32]H. J. Monkhorst and J. D. Pack, Phys. Rev. B **13**, 5188 (1976).
[33]A. Togo and I. Tanaka, Scr. Mater. **108**, 1 (2015).
[34]A. S. Rodin, L. C. Gomes, A. Carvalho, and A. H. Castro Neto, Phys. Rev. B **93**, 045431 (2016).
[35]G. Qin, Z. Qin, W.-Z. Fang, L.-C. Zhang, S.-Y. Yue, Q.-B. Yan, M. Hu, and G. Su, Nanoscale **8**, 11306 (2016).
[36]Q. Wei and X. Peng, Appl. Phys. Lett. **104**, 251915 (2014).
[37]Seixas Research Group (2020). "JanusData," GitHub, see https://github.com/SeixasResearch/JanusData.